Conditional Instabilities of the Greenland Sea

by

James M. Olson
Lieutenant Commander, United States Navy
B.S., University of North Texas, 1982

Submitted in partial fulfillment
of the requirements for the degree of

MASTER OF SCIENCE IN METEOROLOGY AND PHYSICAL OCEANOGRAPHY

from the

NAVAL POSTGRADUATE SCHOOL
September 1992

nclassified

ECURITY CLASSIFICATION OF THIS PAGE

REPORT DOCUMENTATION PAGE

a. REPORT SECURITY CLASSIFICATION nclassified	1b. RESTRICTIVE MARKINGS
a. SECURITY CLASSIFICATION AUTHORITY	3. DISTRIBUTION/AVAILABILITY OF REPORT Approved for public release; distribution is unlimited.
b. DECLASSIFICATION/DOWNGRADING SCHEDULE	
PERFORMING ORGANIZATION REPORT NUMBER(S)	5. MONITORING ORGANIZATION REPORT NUMBER(S)
a. NAME OF PERFORMING ORGANIZATION aval Postgraduate School 6b. OFFICE SYMBOL *(If applicable)* 35	7a. NAME OF MONITORING ORGANIZATION Naval Postgraduate School
c. ADDRESS (*City, State, and ZIP Code*) Ionterey, CA 93943-5000	7b. ADDRESS (*City, State, and ZIP Code*) Monterey, CA 93943-5000
a. NAME OF FUNDING/SPONSORING RGANIZATION 8b. OFFICE SYMBOL *(If applicable)*	9. PROCUREMENT INSTRUMENT IDENTIFICATION NUMBER
c. ADDRESS (*City, State, and ZIP Code*)	10 SOURCE OF FUNDING NUMBERS Program Element No. / Project No / Task No. / Work Unit Accession Number

1. TITLE (*Include Security Classification*)
ONDITIONAL INSTABILITIES OF THE GREENLAND SEA

2. PERSONAL AUTHOR(S) James M. Olson

3a. TYPE OF REPORT	13b. TIME COVERED	14. DATE OF REPORT (*year, month, day*)	15. PAGE COUNT
laster's Thesis	From To	September 1992	58

6. SUPPLEMENTARY NOTATION
he views expressed in this thesis are those of the author and do not reflect the official policy or position of the Department of Defense or the U.S. overnment.

7. COSATI CODES			18. SUBJECT TERMS (*continue on reverse if necessary and identify by block number*)
FIELD	GROUP	SUBGROUP	Oceanography, Depth Dependent Thermal Expansion Coefficient, Neutral Parcel Stability, Deep Convection in the Greenland Sea

9. ABSTRACT (*continue on reverse if necessary and identify by block number*)

This is an examination of the open ocean deep water formation process of the Greenland Sea and how it is effected by the depth dependent thermal expansion coefficient. It is hypothesized that free convection associated with parcel instability is possible because of the increase in the thermal expansion coefficient with pressure in conjunction with requisite ambient temperature and salinity profiles.

Based on the depth dependence of the thermal expansion coefficient, a neutral profile model for parcel instability was formulated and the effects on mixed layer dynamics were investigated. In situ profiles for the wintertime Greenland Sea were examined for potential parcel instabilities. It was shown that only small surface salinity increases associated with freezing could lead to deep penetrative convection. Finally, an analysis was performed for regions of low stability using climatology from the Levitus data set to determine regions most likely for deep convection.

0. DISTRIBUTION/AVAILABILITY OF ABSTRACT	21. ABSTRACT SECURITY CLASSIFICATION	
☒ UNCLASSIFIED/UNLIMITED ☐ SAME AS REPORT ☐ DTIC USERS	Unclassified	
2a. NAME OF RESPONSIBLE INDIVIDUAL oland W. Garwood	22b. TELEPHONE (*Include Area code*) (408) 646-3260	22c. OFFICE SYMBOL OC/Gd

D FORM 1473, 84 MAR 83 APR edition may be used until exhausted
All other editions are obsolete

SECURITY CLASSIFICATION OF THIS PAGE
Unclassified

ABSTRACT

This is an examination of the open ocean deep water formation process of the Greenland Sea and how it is effected by the depth dependent thermal expansion coefficient. It is hypothesized that free convection associated with parcel instability is possible because of the increase in the thermal expansion coefficient with pressure in conjunction with requisite ambient temperature and salinity profiles.

Based on the depth dependence of the thermal expansion coefficient , a neutral profile model for parcel instability was formulated and the effects on mixed layer dynamics were investigated. In situ profiles for the wintertime Greenland Sea were examined for potential parcel instabilities. It was shown that only small surface salinity increases associated with freezing could lead to deep penetrative convection. Finally, an analysis was performed for regions of low stability using climatology from the Levitus data set to determine regions most likely for deep convection.

TABLE OF CONTENTS

I. INTRODUCTION

There are two main regions of deep water formation, near-continent (Antarctic) type and open ocean formation, as discussed in Killworth (1979). The Greenland Sea is the site of formation of the largest volume of deep water in the North Atlantic (Helland-Hansen and Nansen, 1909). Figures (1) and (2) show the Greenland Sea area of interest (Koltermann and Luthje,1989) with the significant topographic features and the schematic circulation.

This paper will examine the open ocean deep water formation process of the Greenland Sea. Of particular interest is how open-ocean deep water formation is influenced by the depth-dependence of the thermal expansion coefficient (α). It is hypothesized that free convection associated with parcel instability is possible because of the increase in the thermal expansion coefficient with pressure in conjunction with requisite ambient temperature and salinity profiles. The thermal expansion coefficient increases with both pressure and temperature. The pressure dependence is more significant for cold polar regions than it is for the deep convection of the Mediterranean, as shown by Garwood (1991). The dependence of α on pressure, or equivalently depth, is a nonlinearity in the equation of state and contributes to a reduction in hydrostatic stability (Carmack and Aagaard, 1973; McDougall, 1987). This reduction in

Figure 1. Greenland Sea Area Chart: Area of interest for conditional instabilities.

Figure 2. Greenland Sea Topography and Circulation: topographic features and schematic of circulation.

stability only occurs when the gradient of temperature is negative for z positive upwards.

Parcel instability may occur if a water parcel that is cold and fresh is displaced downward into water that is warmer and more saline. This greater depth causes increased α for a surface parcel that is displaced downward. For a sufficiently large change in α, the parcel density may be greater than the density of the surrounding water. This parcel would then be unstable and would be accelerated downward by gravity, i.e. a parcel instability would occur.

The traditional explanation of deep-water formation (Nansen, 1906; Mosby, 1959) focused on winter cooling of surface water with the static stability reduced by the cyclonic circulation of the Greenland Sea gyre. Killworth (1979) hypothesized that with progression of winter cooling the depth of the overturning water column increases until top-to-bottom homogeneity is achieved. However, there have been no observations to date that clearly support vertical homogeneity over the whole water column.

Carmack and Aagaard (1973) proposed double diffusion as the cause of the deep water formation. However, Clarke et al. (1990) showed that the double diffusion process can not account for the observed increases in bottom water oxygen concentration over expected values for vertical mixing driven by double diffusion.

Cabbeling (Foster, 1972) and lateral double diffusion have been proposed as mechanisms leading to deep water formation, but neither of these processes are evident in the chimney data presented by Scott and Killworth (1991) (Figure 3). McDougall (1984) showed how diffusion along isopycnal surfaces may lead to water mass formation by both cabbeling and thermobaricity. This study will not focus on isopycnal diffusion, but on surface-driven buoyancy flux.

The Greenland Sea stations of interest are located in the center of the Greenland Gyre (GG) north of the Jan Mayen Current (JMC). Although Killworth (1979) believed that the preconditioning phase does not occur in this region, more recently Clarke et al. (1990) pointed out that parts of the Nordic Seas are considered more susceptible to deep convection than are other areas. The Greenland Sea region circulates cyclonically and is weakly stratified. These conditions permit baroclinic instability (Killworth, 1979), and surface cooling will induce vertical mixing by creating cooler dense water over less dense water. Killworth (1979) hypothesized that the violent mixing initially occurs during winter and only in the top layers. When overturning through the water column results, the entire water column has characteristics that closely resemble those of the deep water. Aagaard and Carmack (1989) found that the deep waters in the Greenland Seas are about the freshest of all waters found in the arctic and subartic. They proposed that the surface freshwater plays a larger role than the intermediate water in the formation process. Gascard (1990) stated that deep convection which leads to deep water formation is a

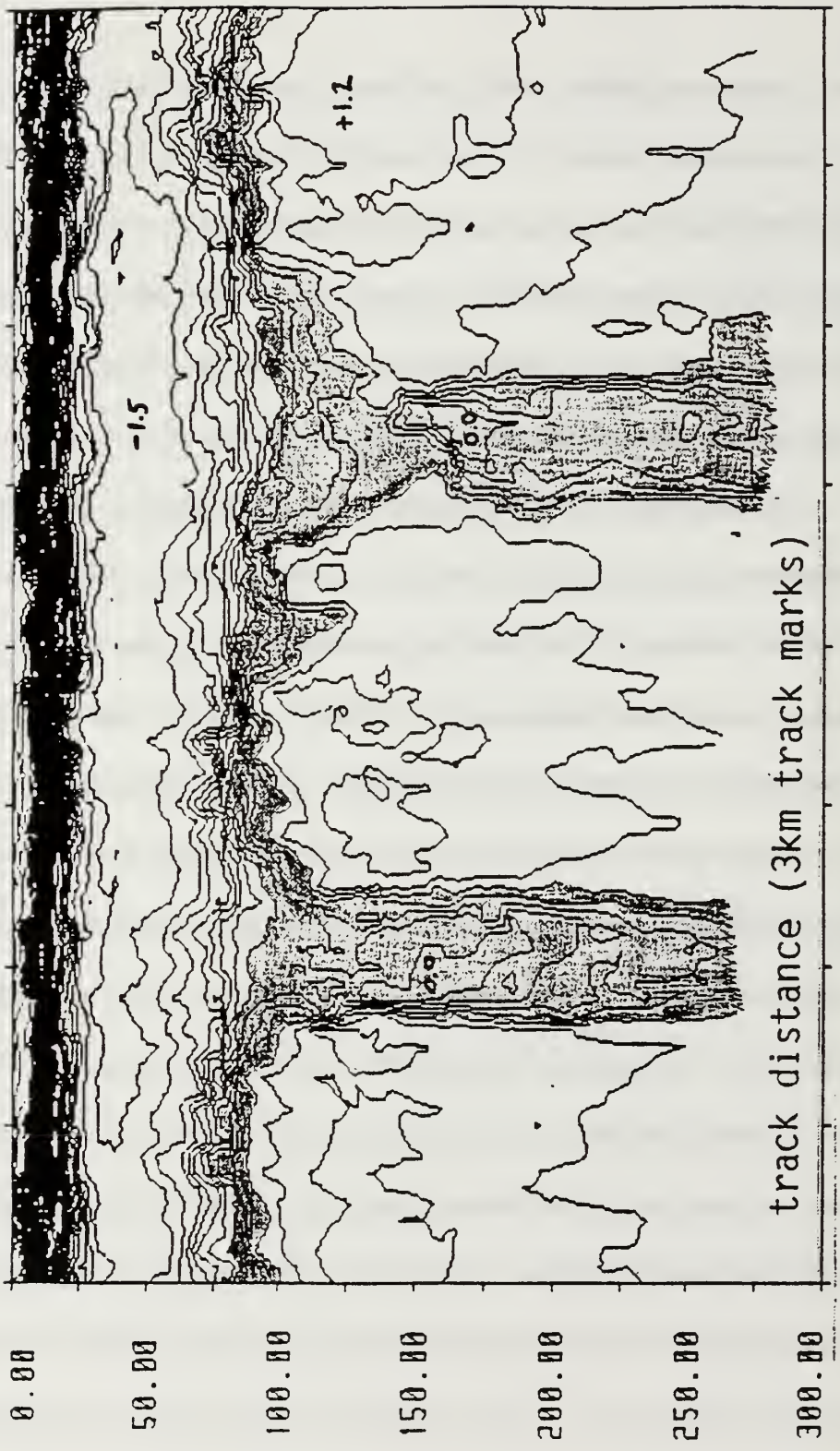

Figure 3. Thermistor Chain Data: Thermistor chain data from the Greenland Sea representing a chimney event.

surface-controlled process involving intermediate and surface waters. The short duration of about one week for chimney events suggested by Rudels (1989) may explain the paucity of observations of convection that reach the bottom in the Greenland Sea. Lazier (1973) showed an isolated example of deep convection in the Labrador Sea reaching approximately 1500 m, but it disappeared within 2-3 days.

Including the increase in the thermal expansion coefficient with pressure, an entrainment model has been developed by Garwood (1991) that includes this nonlinearity in the equation of state. This model predicts greater vertical mixing and penetrative convection than do earlier models because of the nonlinear buoyancy flux enhancement. In the study here, this process will be examined with a conventional one-dimensional model applied to deep oceanic mixing. The investigation will show an increase in vertical turbulent kinetic energy that may enable deep penetrative convection and the hypothesized parcel instabilities leading to formation of deep water.

Before applying the new mixed layer theory, however, a first step in Chapter II was to develop a "neutral parcel" model that predicts a neutrally-stable temperature profile assuming a typical two-layer salinity profile. This profile is neutral to parcel instabilities, i.e. an isolated parcel of water from the mixed layer would have a neutral buoyancy when displaced vertically anywhere in the water column. The surface temperature, surface salinity, mixed layer depth, and the change in salinity at the bottom of the mixed layer are specified.

Then the neutral parcel model diagnoses the change in the temperature at the mixed layer bottom and the change of temperature with depth below the mixed layer. Thus for a given two-layer salinity profile a temperature profile that is neutrally stable for displaced mixed layer parcels is prescribed.

The next step after development of the neutral parcel model is to study the effects of the depth dependent thermal expansion coefficient on mixed layer dynamics. A calibrated Kraus and Turner (1967) model with the depth dependent thermal expansion coefficient is applied to forced and free convection to demonstrate the effect on mixed layer dynamics.

Chapter III will expand in scope from the mixed layer to the entire water column. Parcel instabilities in the water column are examined by moving a parcel from the surface or from within the water column over the entire depth of the water column. Again, the thermal expansion coefficient is considered to be a function of depth and temperatures will be adjusted for heating due to compression by the water column. Surface parcels moved in the water column will then be tested for sensitivity to changes in initial temperature down to freezing and then increases in the initial salinity due to brine injection from ice formation.

Chapter IV explores regional climatology to potential parcel instability, determining regions of lower stability. Regional stability is tested by examining

the change in buoyancy between a surface parcel and the in situ environment at 500 m using climatological temperature and salinity profiles.

II. NEUTRAL PARCEL STABILITY

A. DESCRIPTION

The thermal expansion coefficient, α, is defined as

$$\alpha = -\frac{1}{\rho}\frac{\partial \rho}{\partial \theta} \tag{1}$$

$$\alpha = \alpha_o + ap \tag{2}$$

where ρ is the relative density and θ is the potential temperature. The thermal expansion coefficient increases with pressure (p) as a nearly linear function of pressure (Garwood, 1991). The accurate calculation of α throughout the water column requires knowledge of the ambient salinity and the ambient potential temperature versus pressure throughout the water column. The surface value of the thermal expansion coefficient is determined by

$$\alpha_o = -\frac{1}{\rho}\frac{\partial \rho}{\partial \theta}\Big|_{p=0} \doteq \frac{-\rho(S_o, \theta_o + \Delta\theta, P) + \rho(S_o, \theta_o - \Delta\theta, P)}{2\rho_o \Delta\theta} \tag{3}$$

The values for the density are found using the International Equation of State for seawater (Millero and Poisson, 1981). The neutral-parcel model uses a fixed value of $\Delta\theta$=0.01 C. The centered finite differencing scheme is used along with double precision due to the small differences in density value. An equation similar to (3) is used to calculate alpha at the bottom of the water

column with an adjustment to the potential temperature for the adiabatic temperature increase at the bottom of the water column.

The adjustment for the adiabatic temperature rise is computed using Bryden's (1973) algorithm for adiabatic lapse rate as a function of salinity, pressure, and temperature. By prescribing the surface potential temperature, the salinity and the pressure at the base of the water column, the increase in potential temperature is determined using Newton's convergence technique. The temperature increase due to compression is added to the surface potential temperature to give the corrected potential temperature at the base of the water column. With the calculated temperature and given salinity and pressure at the base of the water column, the bottom value of alpha (α_{bottom}) is calculated using a form of (3). Equation (3) is modified for α_{bottom} by replacing the surface salinity with the bottom values of salinity, pressure, density and corrected potential temperature. Using alpha from the top and the bottom of the water column, the value for (**a**) in (2) is determined using (4). Knowing the constants

$$a = \frac{\alpha(bottom) - \alpha_o}{P_{bottom}} \qquad (4)$$

of (2), the change in the value of alpha from the top to the bottom of the column is specified as a linear function of depth.

The expansion coefficient for salinity is required for the neutral-parcel model to evaluate the change in salinity at the mixed layer interface and in

evaluating the temperature values in the modeled "neutral parcel" water column. The value of β is determined using (5). The expansion coefficient for salinity, β,

$$\beta = \frac{1}{\rho}\frac{\partial \rho}{\partial s} \doteq \frac{0.799}{\rho} \tag{5}$$

is assumed constant throughout the water column. The value of 0.799 psu^{-1} is the average of β values over a 400 bar water column (Gill, 1982).

With the above information, the neutral-parcel model can now be used to prescribe the values for the potential temperature profile as a function of depth or pressure. The physical meaning of the neutral-parcel model is that the profile is stable everywhere for small vertical displacements, with Brunt-Vaisala frequency ($N^2>0$). However, a surface parcel that is moved downward will be perfectly neutral, remaining wherever it is placed with no restoring force. For a neutral buoyancy profile, (6) is used to solve for the potential temperature as a function of depth, (7).

$$\rho(z) = \rho[1 - \alpha(z)[\theta - \theta_o] - \beta[s - s_o]] \tag{6}$$

$$\theta(z) = \theta_o + \frac{\beta \Delta S}{\alpha(z)} \tag{7}$$

Figure (4) shows profile data for station 82 of the Marginal Ice Zone Experiment (MIZEX-87) (Quadfasel et al., 1988). The data from MIZEX-87 was collected during the RV "Valdivia" cruise 54 in March-April 1988 in the

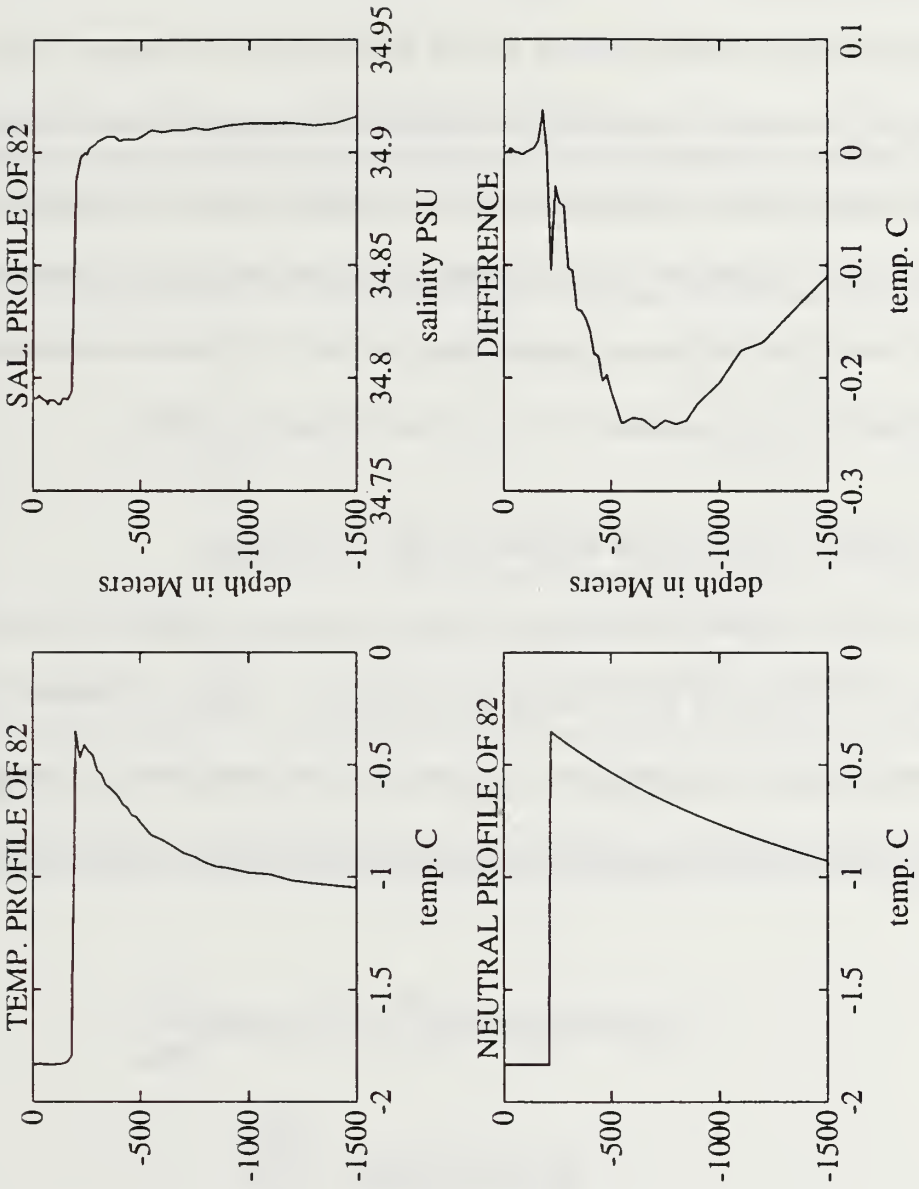

Figure 4. Neutral-Parcel Model Run on Station 82: The top two panels are the T-S profiles of Station 82. The bottom panels show the neutral-parcel model run.

Greenland Sea and the Fram strait. One objective of this cruise was to find and map an active convective element. Station 82 has representative temperature and salinity profiles for the center of the Greenland Gyre. In Figure (4), the lower right plot (DIFFERENCE) represents the difference between station 82's temperature profile and the neutral parcel temperature profile. This "difference" demonstrates how close station 82's temperature profile is to a neutral parcel temperature profile. This also demonstrates that the center of the Greenland Gyre is close to neutral stability.

B. EFFECT OF $\alpha(p)$ ON MIXED LAYER DYNAMICS

To demonstrate, the effect of adding $\alpha(p)$ to a calibrated Kraus and Turner (1967) model, three cases are examined: forced convection, free convection and a combination of forced and free convection. Using the Kraus and Turner model (8) and (9) and the constants listed in Table I determined

$$(-\beta g \Delta S + \alpha g h \Delta T)\frac{\partial h}{\partial t} = c_1 u_*^3 - c_2 \alpha g h \left(\frac{Q_o}{\rho c_p}\right)$$

$$\frac{\partial S}{\partial t} = \frac{(F+E-P)S}{h} - \frac{\Delta S \frac{\partial h}{\partial t}}{h} \qquad (8)$$

$$\frac{\partial T}{\partial t} = \frac{Q_o}{\rho c_p h} - \frac{\Delta T \frac{\partial h}{\partial t}}{h} \qquad (9)$$

TABLE 1. CONSTANTS IN THE PARCEL INSTABILITY MODEL

u_*	1.5 cm/s
g	983 cm/s^2
Δh_o	1800 cm
ΔT_o	$\pm$ 1.52 C
α_o	0.475×10^{-4} s^{-1}
a_1	0.265×10^{-7} $cm^{-1}s^{-1}$
Q_o	-0.005 cal/cm
ρ	1 g/cm^3
c_p	1 cal/g/K

from the NPS mixed layer model (Garwood, 1977) for arctic conditions, the results of forced and free convection for both a constant value of α, and α as a function of depth will be solved numerically and compared. In (8), F is the rate of water freezing, E is the rate of evaporation and P is the rate of precipitation. In (8) and (9), h defines the mixed layer depth, ΔT is the change in temperature at the mixed layer, g is gravity, and $Q_o/\rho c_p$ is the downward surface temperature flux. Constants c_1 and c_2 are dimensionless model constants.

The cooling case ($Q_o < 0$) with continued deepening of the mixed layer over time will be considered first. The left hand side of (8) is the rate turbulent kinetic energy (TKE) is converted to potential energy (PE) by entrainment (layer deepening). The first term on the right hand side of (8) is the generation rate of the TKE by wind stirring minus viscous dissipation. The second term is damping ($Q_o > 0$) of TKE by surface heating or free convection production ($Q_o < 0$) of TKE by surface cooling. The left hand side of (9) is the rate of change of the temperature at the bottom of mixed layer. The first term on the right hand side of (9) is the surface heating and the second term is the entrainment heat flux, with a mixed layer temperature decrease(increase) if ΔT is positive(negative).

For case 1, forced convection (Q_o= 0), the wind forcing is the only source of turbulent kinetic energy. For this case (8) and (9) simplify to (10) and (11).

$$\frac{\partial T}{\partial t} = -\frac{\Delta T}{h}\frac{\partial h}{\partial t} \tag{10}$$

$$\frac{\partial h}{\partial t} = \frac{c_1 u_*^3}{\alpha g h \Delta T - \beta g \Delta S} \tag{11}$$

Note that $h\Delta T$ equals a constant:

$$\Delta T = T - T(Z = -h)$$

$$\frac{\partial \Delta T}{\partial t} = \frac{\partial T}{\partial t} - \frac{\partial T}{\partial t}(-h)$$

$$\frac{\partial T}{\partial t}(-h) = 0$$

$$\frac{\partial T}{\partial t} = -\frac{\Delta T}{h}\frac{\partial h}{\partial t}$$

$$h\frac{\partial \Delta T}{\partial t} + \Delta T\frac{\partial h}{\partial t} = 0$$

$$\frac{\partial}{\partial t}(h\Delta T) = 0$$

For α constant over depth and a positive(negative) ΔT, integrating (11) from h_o to h will result in a linearly increasing(decreasing) mixed layer depth as a function of time.

With the same initial conditions, (11) becomes (12) if α is depth dependent. Integrating from h_o to h results in (13). Figure (5) shows the deepening(shallowing) of the mixed layer depth for constant α and depth dependent α versions of case 1. The mixed layer deepening(shallowing) is slowed over a one day period when α is depth dependent. Furthermore, the

$$\frac{\partial h}{\partial t}=\frac{c_1 u_*^3}{g h_o \Delta T_o}\left(\frac{1}{\alpha_o - a_1 z}\right) \tag{12}$$

$$h-h_o=\frac{c_1 u_*^3}{g h_o \Delta T_o}\frac{t}{(\alpha_o + a_1 h)} \tag{13}$$

depth dependent α causes a nonlinear change in depth of the mixed layer as noted by the slight curvature of the dotted line for positive ΔT and the dashed line for negative ΔT in Figure (4).

Case 2, free convection (u.= 0), the condition of surface cooling ($Q_o < 0$) for a constant α and $\alpha(z)$ are compared. Using the Kraus and Turner model on the free convection case results in (14). Notice in (14) that α appears in both

$$\frac{\partial h}{\partial t}=\frac{-c_2 \alpha g h\left(\frac{Q_o}{\rho c_p}\right)}{\alpha g h \Delta T} \tag{14}$$

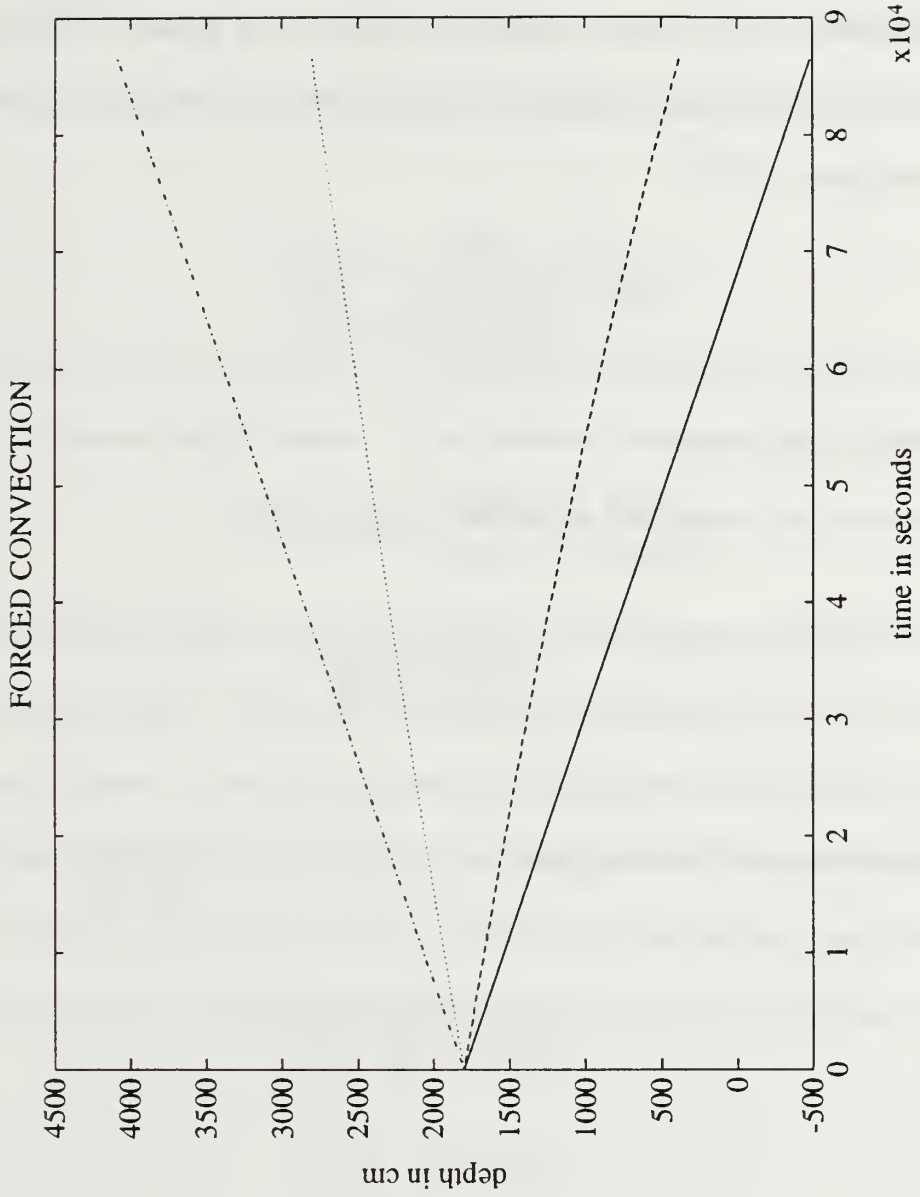

Figure 5. Case 1: Forced convection mixed layer deepening(shallowing), constant α is the dot-dashed(solid) line and $\alpha(z)$ is the dotted(dashed) line.

the numerator and the denominator. It is not eliminated because α now has different rates at the top and bottom of the mixed layer. The first term on the right hand side of (15) is the turbulent heat flux at the surface, $\overline{T'w'}\Big|_0$. The second term on the right hand side of (15) is turbulent heat flux at the bottom of the mixed layer, $\overline{T'w'}\Big|_h$.

$$h\frac{\partial T}{\partial t}=\frac{Q_o}{\rho c_p}-\Delta T\frac{\partial h}{\partial t} \tag{15}$$

When $\alpha$was assumed constant, the α values in the numerator and denominator can be divided out which reduces (14) to

$$\Delta T\frac{\partial h}{\partial t}=-c_2\frac{Q_o}{\rho c_p} \tag{16}$$

And recall from earlier that at z=-h, $\frac{\partial \Delta T}{\partial t}=\frac{\partial T}{\partial t}$

Then,

$$h\frac{\partial \Delta T}{\partial t}+\Delta T\frac{\partial h}{\partial t}=\frac{-c_2Q_o}{\rho c_p}$$

$$\frac{\partial}{\partial t}(h\Delta T)=\frac{-c_2Q_o}{\rho c_p}$$

Now integrating from h_o to h results in $h\Delta T-h_o\Delta T_o=\frac{-c_2Q_o}{\rho c_p}t$

Solving (16) numerically gives solutions in Figure (6).

For the depth dependent α case, substitute $\alpha=\alpha_0-a_1z$ into (14). The value of α in the numerator will be α_0 since it is the surface flux component. The denominator α value becomes $\alpha_0+ a_1 h(t)$ at the bottom of the mixed layer ($z = -h$). Using these substitutions and solving at $z = -h$ yields,

$$\frac{\partial}{\partial t}(h\Delta T)=\frac{-c_2Q_0}{\rho c_p}\left(\frac{\alpha_0}{\alpha_0+a_1h(t)}\right)$$

Integrating from h_0 to h gives (17). Figure (6) shows that the mixed layer is

$$h\Delta T-h_0\Delta T_0=\frac{-c_2Q_0}{\rho c_p}\int\frac{\alpha_0}{\alpha_0+a_1h(t)}dt \qquad (17)$$

deepening(shallowing); however, the rate of deepening(shallowing) is much slower than in case 1. Note that the deepening(shallowing) is much slower than that in case 1. For the $\alpha(z)$ case, the magnitude of reduction in the rate of mixed layer deepening(shallowing) is smaller than that in the forced convection case. Thus the results show that as in the forced convection case, the slowing of the mixed layer deepening(shallowing) is caused by the increase in α with time.

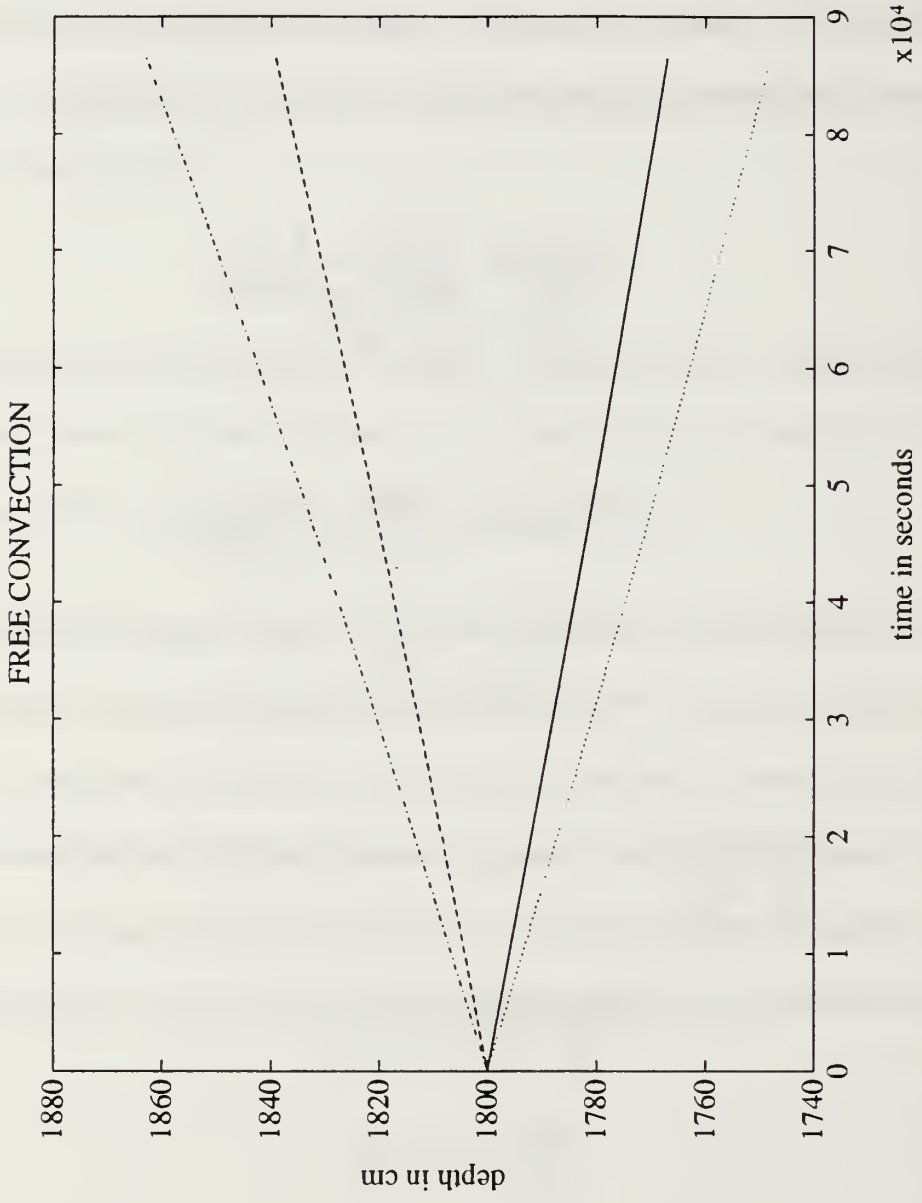

Figure 6. Case 2: Free convection mixed layer deepening(shallowing), constant α is the dot-dashed(dotted) line and $\alpha(z)$ is the dashed(solid) line.

Cases 1 and 2 were a simple analysis of how the Kraus an Turner (1967) model was effected by simply plugging in $\alpha(z)$. Case 3 will examine how the Kraus an Turner (1967) model is effected when $\alpha(z)$ is considered in the derivation of (8) and (9). For case 3, the combined effects of both forced and free convection ($Q_o < 0$ and $u_* \neq 0$) are examined. The first term on the right hand side of (8), generation rate of wind stirring minus viscous dissipation, can be rewritten in terms of turbulent heat flux as shown in (18). The top line of (8) can be rewritten as (19) using form shown in (18), the generation rate of TKE balance by the vertically integrated buoyant dampening.

$$c_1 u_*^3 = \frac{1}{h}\int_{-h}^{o} \alpha g \overline{T'w'} dz \tag{18}$$

$$\alpha g h[\Delta T \frac{\partial h}{\partial t} + c_2 \frac{Q_o}{\rho c_p}] = \frac{1}{h}\int_{-h}^{o} \alpha g \overline{T'w'} dz \tag{19}$$

The turbulent heat flux is a function of the depth and is written in the form Multiply the turbulent heat flux by αg, substitute in the expressions for the

$$\overline{T'w'}(z) = \overline{T'w'}(0)(1 + \frac{z}{h}) - \overline{T'w'}(-h)(\frac{z}{h}) \tag{20}$$

surface turbulent heat flux and the turbulent heat flux at the bottom of the mixed layer, and integrate over the depth of the mixed layer. These operations

result in (21). The left hand side of (21) is the integral average of the buoyancy flux over the water column. The first term on the right hand side is the buoyancy flux component due to the net downward temperature flux. The second term is the buoyancy flux component due to the bottom heat flux.

$$\int_{-h}^{o}\alpha g\overline{T'w'}dz=\int_{-h}^{o}\alpha g(1+\frac{z}{h})(-\frac{Q_o}{\rho c_p})dz+\int_{-h}^{o}\alpha g(\frac{z}{h})(\Delta T\frac{\partial h}{\partial t})dz \qquad (21)$$

For constant α, we can reduce (21) by dividing out the gravity and solving the integral to give

$$\frac{1}{h}\int_{-h}^{o}\alpha\overline{T'w'}dz=[-\frac{Q_o}{\rho c_p}-\Delta T\frac{\partial h}{\partial t}]\frac{\alpha_o}{2} \qquad (22)$$

For the depth dependent α, we will substitute into (21) the form $\alpha = \alpha_o - a_1 z$ from (2):

$$\int_{-h}^{o}\alpha g\overline{T'w'}dz$$

$$=\int_{-h}^{o}g(\alpha_0-a_1z)(1+\frac{z}{h})(-\frac{Q_o}{\rho c_p})dz$$

$$+\int_{-h}^{o}g(\alpha_0-a_1z)(\frac{z}{h})(\Delta T\frac{\partial h}{\partial t})dz$$

Expanding the integral gives (23).

$$= -\frac{Q_o}{\rho c_p}\int_{-h}^{o}[\alpha_o - a_1 z + \alpha_o \frac{z}{h} - a_1 \frac{z^2}{h}]dz + \Delta T \frac{\partial h}{\partial t}\int_{-h}^{o}[\alpha_o \frac{z}{h} - a_1 \frac{z^2}{h}]dz \qquad (23)$$

Simplify (23) results in,

$$= -\frac{Q_o}{\rho c_p}[\alpha_o z - \frac{a_1}{2}z^2 + \frac{\alpha_o}{2}\frac{z^2}{h} - \frac{a_1}{3}\frac{S^3}{h}]_{-h}^{o} + \Delta T \frac{\partial h}{\partial t}[\frac{\alpha_o}{2}\frac{z}{h} - \frac{a_1}{S}\frac{z^3}{h}]_{-h}^{o}$$

Evaluating this expression gives (24); the buoyancy flux components due to net downward temperature flux and bottom heat flux.

$$= g\frac{Q_o}{\rho c_p}[\frac{\alpha_o}{2} + \frac{a_1}{6}h] - g\Delta T \frac{\partial h}{\partial t}[\frac{\alpha_o}{2} + \frac{a_1}{3}h] \qquad (24)$$

In comparing (22) and (24), notice that the depth dependent α causes an increased weighting to both the temperature and bottom heat flux components. Another difference is the weighting between the two fluxes. The bottom heat flux has a larger weight which makes it a larger reduction(addition) in the buoyancy flux due to the net downward temperature flux, depending on whether ΔT is positive or negative. This shows that the depth dependent α causes the mixed layer to deepen(shallow) at a slightly slower rate for a positive(negative) ΔT than what is found for constant α.

III. TEST OF PARCEL INSTABILITY THEORY

A. WATER COLUMN INSTABILITIES

The response of the mixed layer to the nonlinear effects of $\alpha(z)$ was investigated in the previous section, but the possibility of instability below the mixed layer needs to be considered. Figure (3) depicts Scott and Killworth's (1991) thermistor chain data from a track between Greenland and Iceland. The temperature contours show the existence of two chimneys below the surface. The chimneys represent events that are clearly below the surface boundary layer. Are there features analogous to cumulus cloud formation in the atmosphere? Riehl (1979) describes how atmospheric deep convection in the tropics requires only a small percentage of the region to be conditionally unstable. Is this the same situation seen in deep chimney oceanic convection? Scott and Killworth (1991) hypothesized that the chimneys in Figure (3) are decoupled from the surface. A chimney could be coupled with the surface if it were created by a small instability in a region of conditional instability. A small instability from the surface would not be very evident once the chimney event started. Thus what looks decoupled after the chimney is developed may not show how the surface initiated the event.

To determine how an instability in a region of conditional instability relates to our neutral-parcel instabilities, the model is applied to station data in the

Greenland gyre. By displacing a surface parcel downward in the water column, the possibility of parcel instability is explored. The surface parcel may be cooled and its salinity may also be changed by freezing. The effect on stability for such alleged surface parcels is also examined. This procedure demonstrates what changes in a surface parcel can cause instability or make the parcel neutrally stable/unstable and therefore favorable for a convective event.

B. MODEL DESCRIPTION

To investigate the possibility of parcel instabilities using in situ data, temperature and salinity values from station 44 of MIZEX (Quadfasel et al., 1988) are applied to the parcel instability model. The temperature and salinity data is used in the Millero and Poisson (1981) equation of state to obtain density values throughout the water column. The temperature is adjusted for the heat of compression with increasing depth by using Bryden's (1973) algorithm to obtain potential temperature (degrees C) as a function of salinity (psu), temperature (C) and pressure (bars).

The in situ density is calculated at each level of the temperature and salinity profile. Then moving the surface parcel down the water column profile, the temperature is adjusted for compression at each new pressure level using the Bryden algorithm. With the compression-adjusted surface temperature and surface salinity, the density is calculated for the surface parcel at each pressure

level. Each level has an in situ density and a density for the surface parcel moved to that level. The change in density is found at each level by

$$\Delta \rho_s = \rho_{insitu} - \rho_{sfcparcel}$$

When $\Delta\rho_s$ is negative, the surface parcel would be unstable (more dense) compared to its surroundings and would accelerate downward by gravity until it reached a depth with equal density or until it encountered the bottom.

Station 44 will be examined to determine if the situation described above ever occurs. The results are seen in Figure (7), a plot of depth versus $\Delta\rho$. The solid line shows the non-compression adjusted temperature values for the change in density at each level as depth increases. The dashed line shows the adiabatic temperature adjusted surface parcel changes in density as depth increases. The profiles do not exhibit any parcel instabilities for the displaced surface parcel since the values of $\Delta\rho$ never become negative. Figure (7) also shows that the temperature adjustment is a stabilizing effect for the profile; the adiabatic temperature corrected $\Delta\rho$ curve is more positive through the water column.

1. SENSITIVITY TO DEPTH

The procedure described is then modified to begin with a parcel at the bottom of the mixed layer vice a surface parcel. No parcel instabilities were noted. Other levels are also examined, and no parcel instabilities were discovered. Figure (8) is an example of this procedure. The dot-dash line

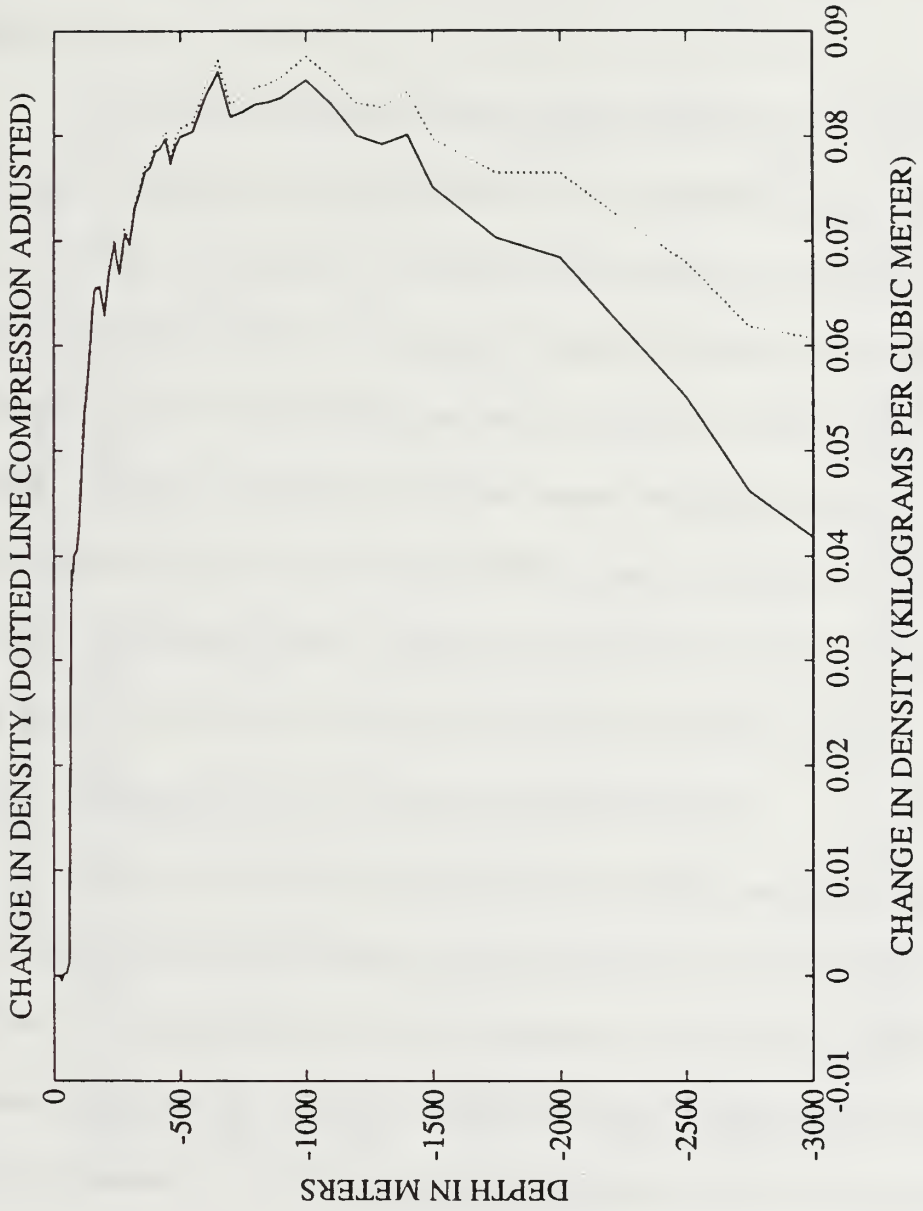

Figure 7. Change in density curves for Station 44: The dotted curve represents adiabatic temperature adjustment. The solid curve is not adiabatic temperature adjusted.

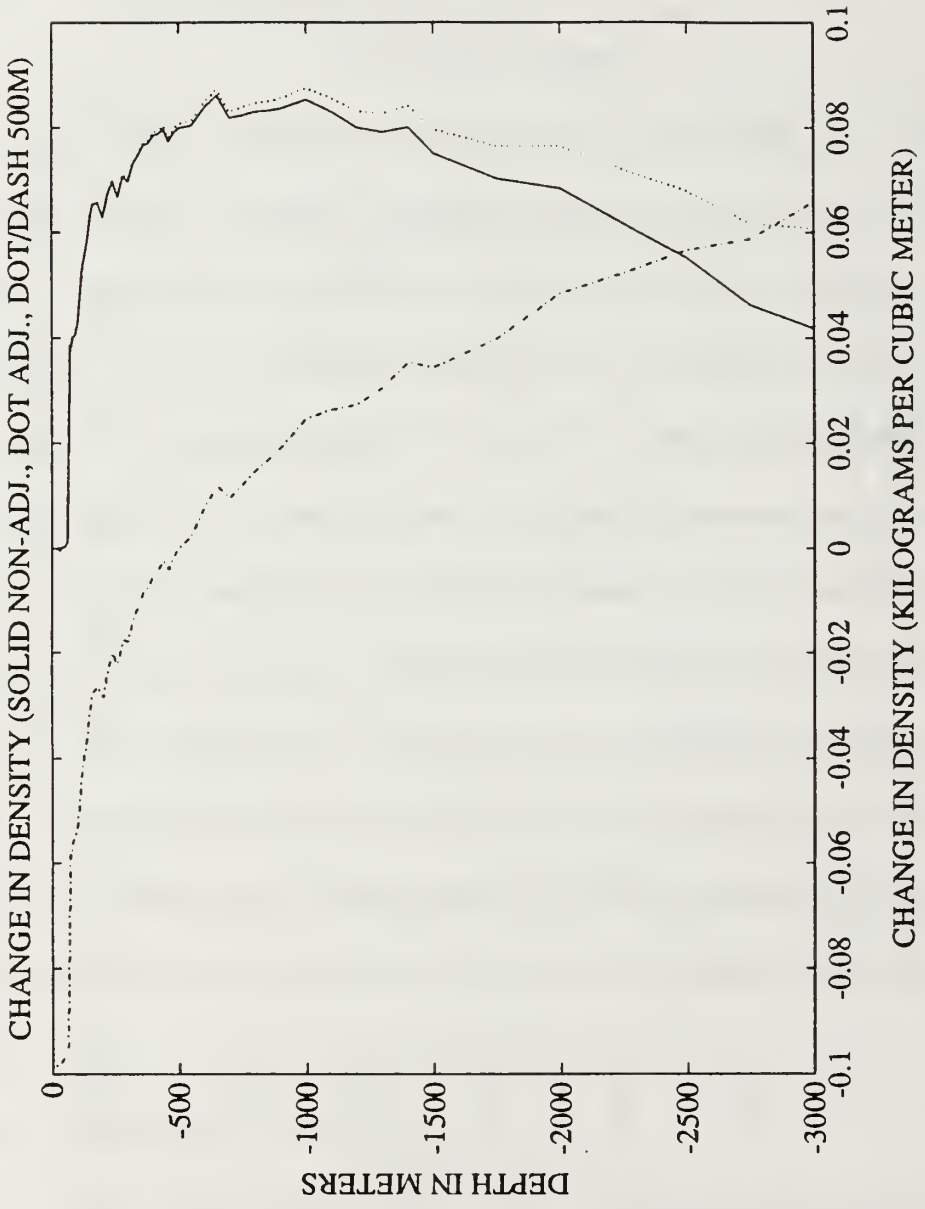

Figure 8. Change in density curve: Testing for depth sensitivity, solid being non-adiabatic, dotted being adiabaticly adjusted and dot-dash is a 500 m parcel moved in the water column.

shows a parcel from 500 meters depth moved to the surface and then moved down the water column. Below 500 meters the 500 meter parcel never became unstable.

It is worth noting that Gascard (1991) stated that chimney formation only occurs were the overall stratification can be destabilized and destroyed from the interior. He further stated that vertical mixing by turbulent entrainment triggered from the surface is ineffective. Figure (8) shows an example of a test for destabilization of the stratification from the interior, i.e. 500 meters in this example. However, looking at the above parcel instability model for the data in the Greenland Sea given by Gascard (1991) shows no parcel instabilities using water from intermediate levels. Figure (9) demonstrates how a 1000 meter parcel moved in the water column did not cause instability either.

2. SENSITIVITY TO SURFACE TEMPERATURE

The next test was to assume that the surface was cooled in steps down to the freezing temperature by either heat loss to the atmosphere or by advection. By using Millero's (1978) equation for the freezing point of seawater, the maximum amount of cooling that could be imposed on the surface is calculated. At station 44, the surface temperature was already -1.797 C and could only be cooled by 0.1 C to reach the freezing point.

The first step is to apply the parcel instability model with station 44's original surface temperature. Each consecutive test is applied to the same station 44 water column profile but with the surface parcel temperature

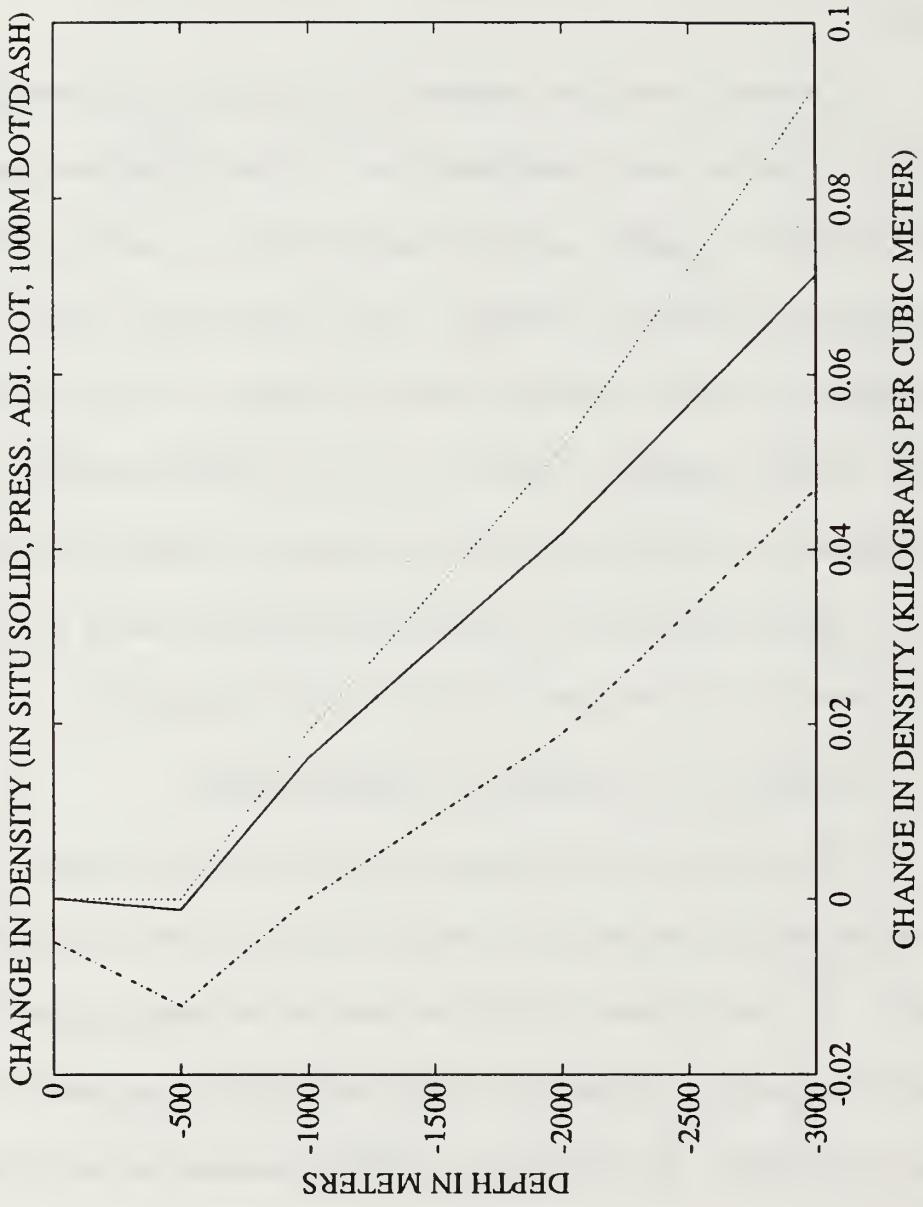

Figure 9. Change in density: Test of Gascard's Greenland Sea data for internally caused instabilities.

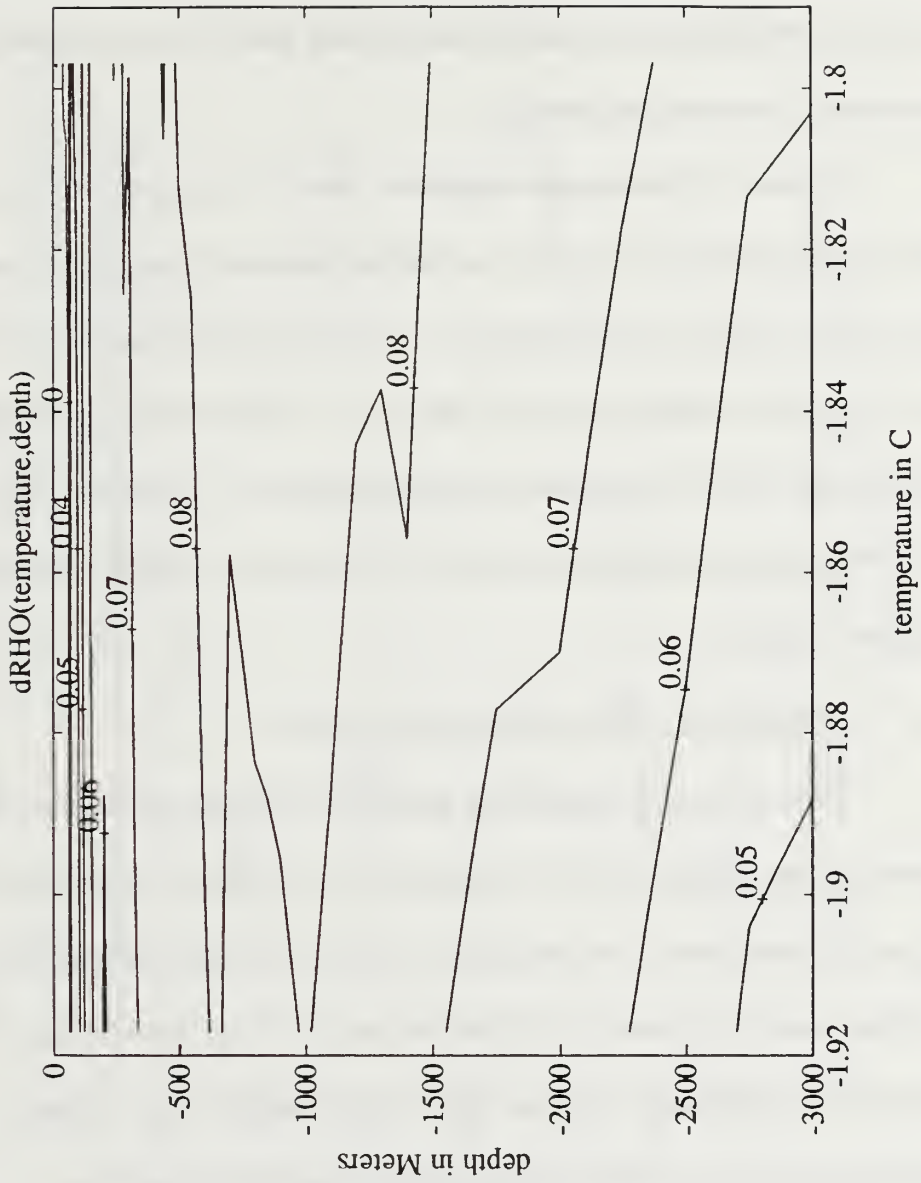

Figure 10. Contour of $\Delta\rho(\theta,Z)$: Sensitivity to reducing surface temperature to freezing.

reduced by 0.02 C at the start of each iteration until the freezing temperature was reached. Figure (10) shows the contours of $\Delta\rho(\theta,z)$. Viewing Figure (10) from right to left shows the result of decreasing station 44's surface parcel temperature to the freezing point.

Figure (11) shows an expanded view of the upper 750 m for the same contour intervals. The only instabilities demonstrated are in the upper 50 m of the water column, the mixed layer. One interesting feature to note is a zone of maximum stability between 500 m and 1500 m that is strongest at the original surface parcel temperature and becomes less dominant as surface parcel temperature approaches freezing. This can is evident from the 0.08 $\Delta\rho$ contour in Figure (11).

3. SENSITIVITY TO SURFACE SALINITY

With no parcel instabilities apparent in the water column when the temperature was reduced to the freezing point, the effects of surface salinity changes are examined. An increase in salinity is associated with freezing after the surface water is cooled to the freezing point. Then the change in salinity (δS) times the thickness of the ice (h) is proportional to the change in the ice thickness (δh) times the difference in surface salinity (S) and ice salinity (S_i),

$$\delta S * h \approx \delta h * (S - S_i)$$

The salinity of the ice is approximated with Maykut's (1985) ice salinity data.

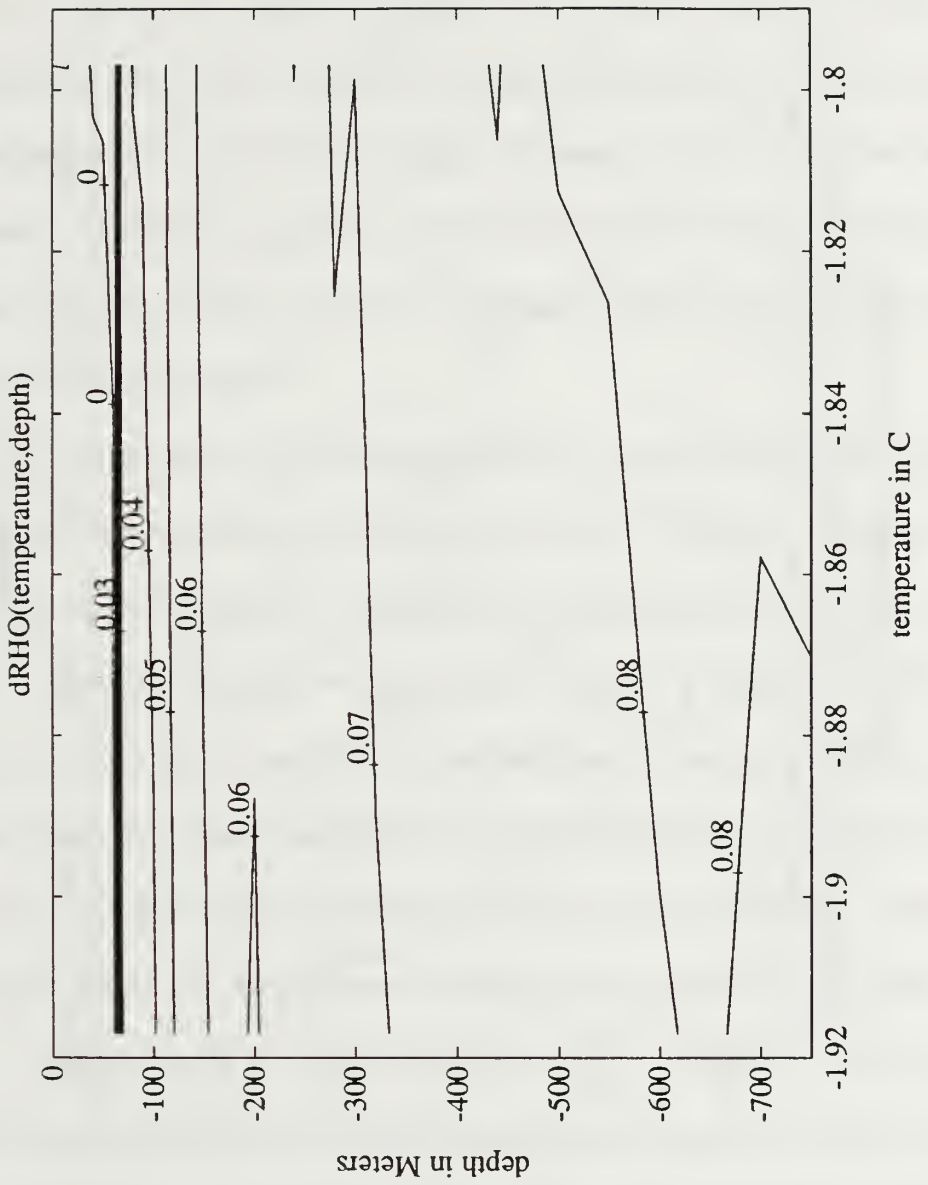

Figure 11. Contour Plot of $\Delta\rho(\theta,Z)$: Expanded view of the upper 750 meters of sensitivity to reducing surface temperature to freezing.

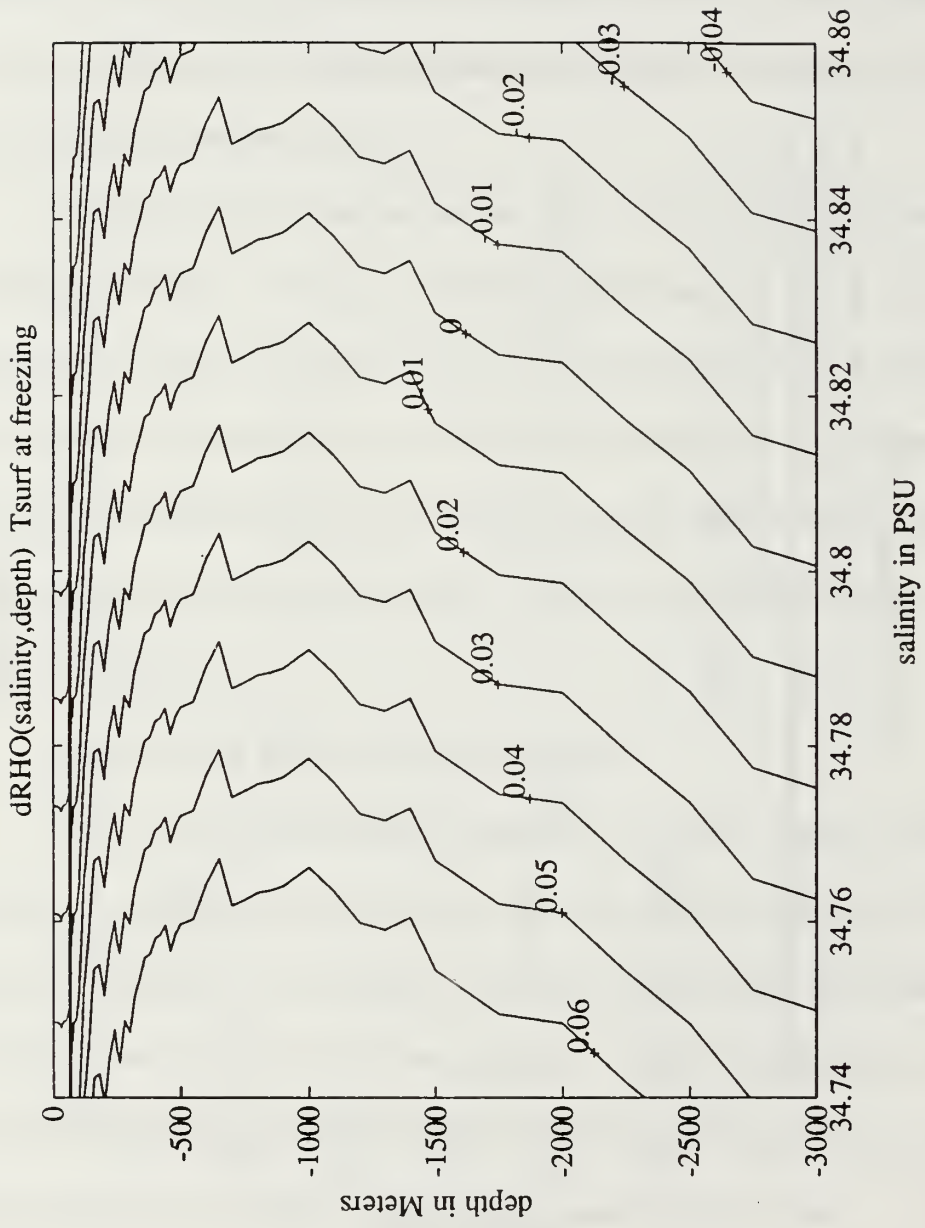

Figure 12. Contours of $\Delta\rho(S,z)$: Sensitivity to increasing salinity by .02 psu with the surface temperature at freezing.

An ice salinity value of 12 psu for first year ice of initial thickness at 5 cm or less will give approximately 0.1 psu increase in salinity for 1 cm of ice growth at the surface of the water column. This does not account for the salinity increases due to mixed layer turbulent mixing or advection of colder more saline water into the surface water. Anderson's (1961) data for ice growth rate gives a 10 cm/day ice growth rate for a storm with air temperatures at -40 C. Thus an increase of 0.1 psu for the surface water is reasonable to use in the parcel instability model.

Solving the parcel instability model for the surface parcel at freezing temperature and increasing the salinity by 0.1 psu in 0.02 psu increments gives the contour plot of figure (12). The graph is salinity vs. depth, plotting the change in density between the surface parcel moved to depth as salinity increases by 0.02 psu increments, $\Delta\rho$(salinity,depth). As the salinity is increased from its original value at the surface of 34.74 to 34.80 psu and greater, the parcel instability (negative values of $\Delta\rho$) are predicted. Also, values greater than 34.84 psu show parcel instability to the bottom of the water column. The second to the last iteration (second to last contour on the right) shows the neutral stability curve for a parcel moved from the surface to depth without any change in the density between the surface parcel at the freezing point and the in situ water density.

Figure (13) shows an expanded view of the upper 750 m for the same contour intervals. This shows how the mixed layer instability grows very

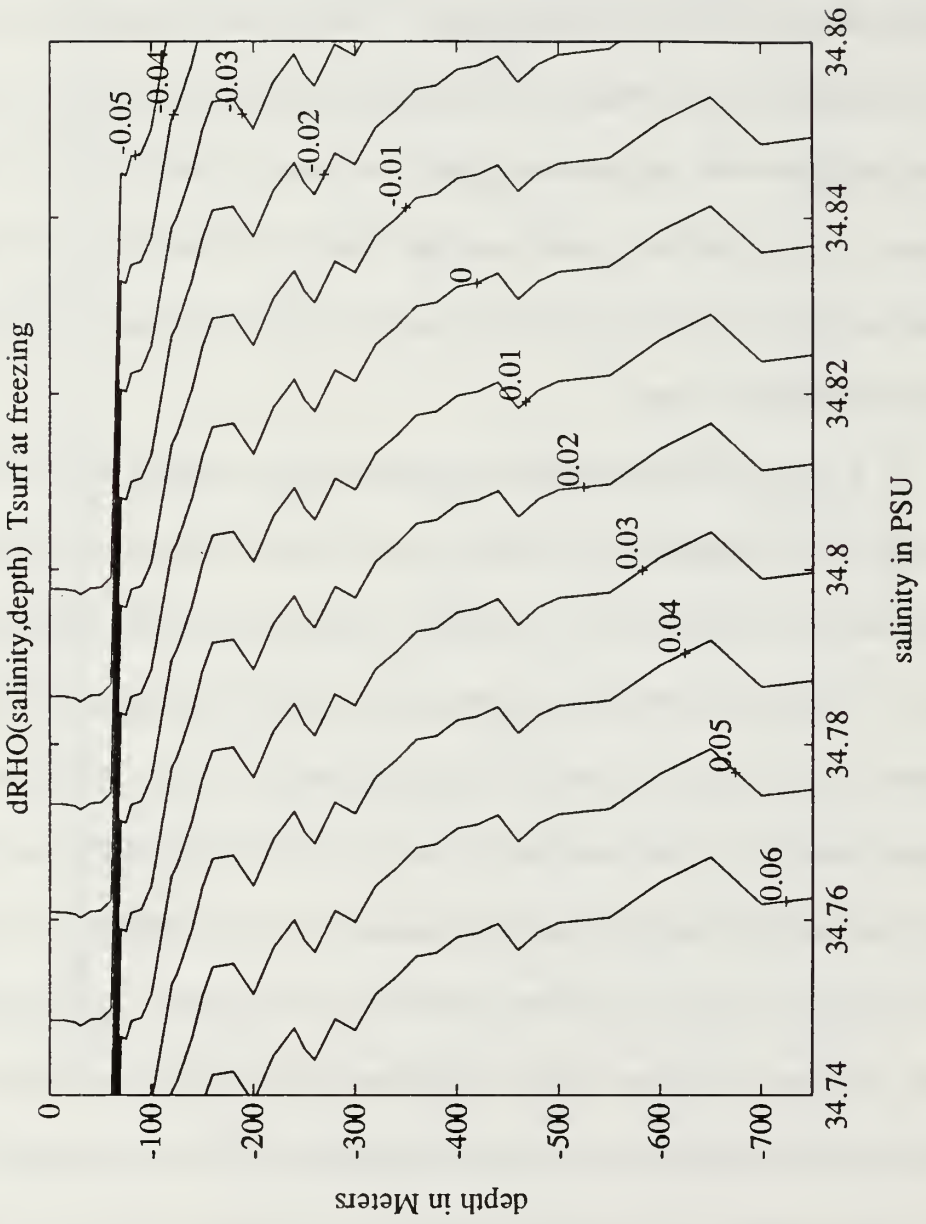

Figure 13. Contour Plot of $\Delta\rho(S,z)$: Expanded view of upper 750 meters, sensitivity to increasing salinity with surface temperature at freezing.

quickly from the onset of the salinity increase. Examining the values of instability near the salinity value of 34.76 psu shows at what value parcels should "break out" of the mixed layer in deep convection events. Thus the model demonstrates that a parcel instability can occur for the station 44 profile provided that the surface is cooled to freezing and as little as 1 cm of ice forms. The salinity injection and surface temperature changes at the surface can create a parcel instability that can cause convection to the bottom of the water column.

IV. CLIMATOLOGY

A. CLIMATOLOGY AND PARCEL INSTABILITY

Is there a region in the Greenland sea that can be considered preferential for parcel instability events leading to chimneys? With the assumption that parcel instabilities depend on a depth dependent thermal expansion coefficient the Levitus(1982) Climatological Atlas of the World Oceans is used to investigate the Greenland Sea. The Levitus (1982) data set contains temperature and salinity at standard oceanographic observation levels on a one degree latitude and longitude grid for the world oceans. The data are averages of objectively analyzed station data, mechanical bathythermograph and expandable bathythermograph between the surface and a maximum depth of 5500 meters. Annual and seasonal data were provide, but only the winter season data is used for the parcel instability analysis here.

B. CLIMATOLOGICAL MODEL TEST

Again using the depth dependent thermal expansion coefficient and the principles of the parcel instability model, the temperature and salinity values from 55 N to 85 N in latitude and 5 E to 20 W in longitude will be used to determine the stability of the region. The surface values of temperature and salinity from the data set do not represent a very realistic mixed layer due to

the averaging process, but it is assumed they provide an adequate first guess field. A depth of 500 m will be the comparison depth for the instability test. This depth is used to help cover the largest area of the data set without being bottom limited. The 500 m depth is also a reasonable chimney depth evident in various data sets.

The model will use (25) to determine the buoyancy jump (Δb) as a function of the 500 m depth to create a grid of the change in buoyancy (Δb)

$$\Delta b = g(\alpha_{500}(T_{surf} - T_{500}) - \beta(S_{surf} - S_{500})) \qquad (25)$$

values to contour. The values subscripted with 500 indicate the value at 500 m and the subscript surf indicates the surface value. Again, in this test β will be kept constant.

Figure (14) represents the Δb values plotted on the latitude and longitude grid. The area encircled by the 0.1 cm/s^2 contour represents an area close to neutral stability. Comparison of this area to the charts in Figures (1) and (2) show that this is highly correlated to the central region of the Greenland Gyre. The areas on Figure (14) without a contour value represent land or the water depth was too shallow for comparison with the 500 m depth.

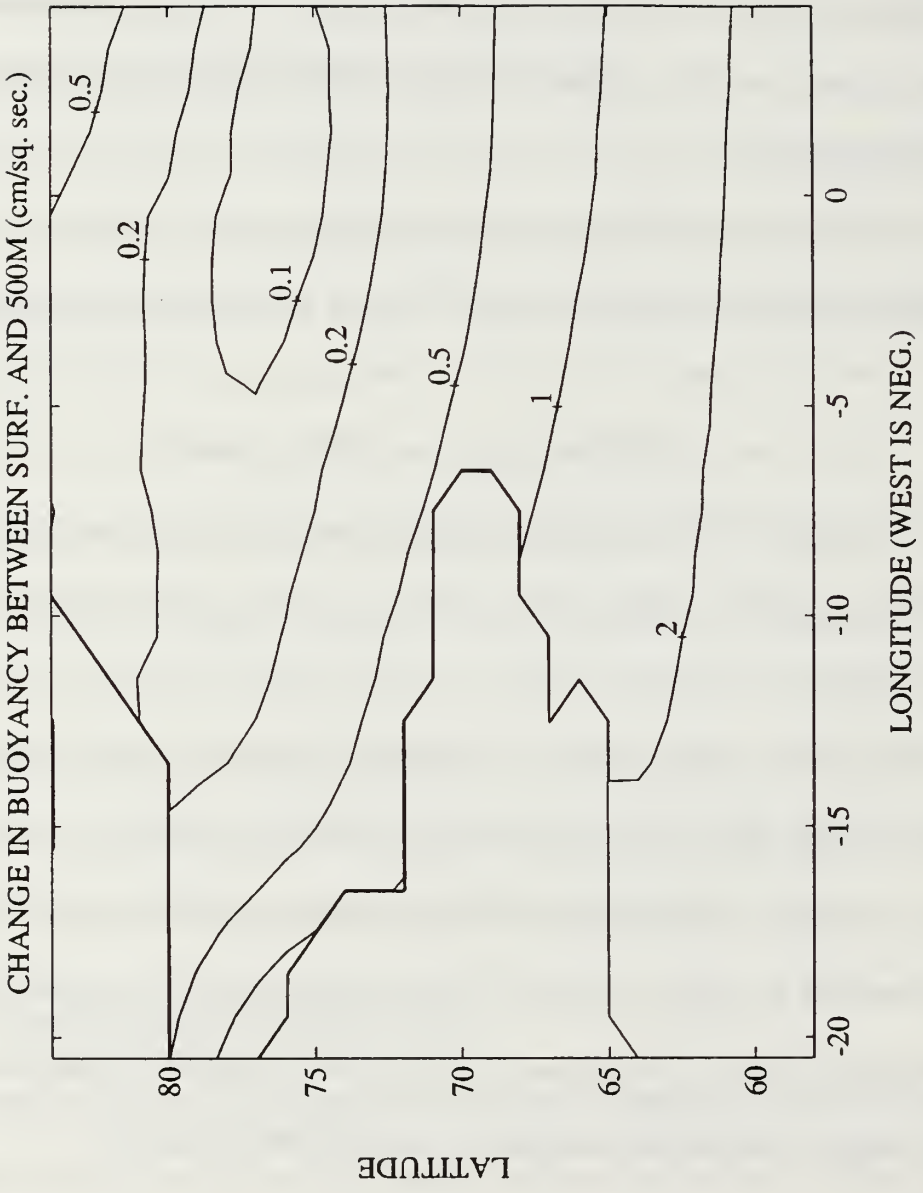

Figure 14. Contoured Plot of Change in Buoyancy: Contours of the Δb between the surface values and a depth of 500 meters.

This instability test supports the theory that the Greenland Gyre is the most likely candidate for chimney formation in the Greenland Sea region. It helps provide a bounds for further data collection and observations of chimney events.

V. SUMMARY

This study has (1) investigated the dynamics of a neutral-parcel model with a depth varying thermal expansion coefficient (α), and (2) tested for parcel instability in the Greenland Sea, using both actual profiles and climatological data.

In the neutral-parcel model, the effects on mixed layer dynamics for forced and free convection and the combination of both were analyzed for what added dynamical effect the depth dependent $\alpha(z)$ had on the mixed layer in each test. The depth dependent $\alpha(z)$ changes significantly mixed layer deepening. For all three cases of convection, depth dependent $\alpha(z)$ caused the mixed layer to deepen(shallow) at a slower rate given a positive(negative) ΔT than what was found for a constant α.

The parcel instability model using $\alpha(z)$ and adiabatic temperature increases due to parcel movement down the water column was tested for sensitivity to parcels displaced from interior depths, sensitivity to reducing the surface temperature to freezing and sensitivity to increases in the surface salinity. Gascard's (1991) destabilization from the interior could not be supported using the parcel instability model, demonstrated by the test for depth sensitivity using data from Gascard (1991). Reducing the surface temperature to freezing showed the onset of freezing reduced the stability and brought it

closer to neutral stability. Cooling surface temperature to freezing did not by itself lead to a state of instability for most of the profiles tested. When the surface was at freezing and enough ice formation occurred, then the increase in salinity resulted in the possible onset of parcel instability.

Using the depth dependent thermal expansion coefficient and adiabatic temperature increases, an assessment of the possible instability in the climatological data of the Greenland Sea was made. The area of least stability for this test was the center of the Greenland Gyre.

LIST OF REFERENCES

Aagaard, K. and E.C. Carmack, 1989: "The role of sea ice and other fresh water in the Arctic circulation." J. Geophys. Res., **94**, 14, 485.

Anderson, D.L., 1961: "Growth rate of sea ice." J. Glaciol., **3**, 1170-1172.

Bryden, H.L., 1973: "New polynomials for thermal expansion,diabatictemperature gradient and potential temperature gradient of sea water." Deep Sea Research, **20**, 401-408.

Carmack, E.C., and K. Aagaard, 1973: "On the deep water of the Greenland Sea." Deep Sea Research, **20**, 687-715.

Clarke, R.A. et al., 1990: "The formation of Greenland Sea deep water: Double diffusion on deep convection?" Deep SeaResearch, **37**, 1385-1424.

Foster, T.D., 1972: "An analysis of the cabbeling instability in seawater." J. Phys. Oceanogr., **2**, 294-301.

Garwood, R.W., Jr., 1991: "Enhancements to deep turbulent entrainment." *Deep Convection and Deep Water Formation inthe Oceans*. Ed. P.C. Chu and J.C. Gascard. Elsevier Science Publishing Company Inc., Amsterdam, The Netherlands, 197-213.

Garwood, R.W., Jr., 1977: "An oceanic mixed layer model capable of stimulating cyclic states." J. Phys. Oceanogr., **19**, 901-916.

Gascard, Jean-Claude, 1991: "Open ocean convection and deep water formation revisited in the Mediterranean, Labrador, Greenland and Weddell seas." *Deep Convection and Deep Water Formation in the Oceans*. Ed. P.C. Chu and J.C. Gascard. Elsevier Science Publishing Company Inc., Amsterdam, The Netherlands, 157-181.

Gascard, Jean-Claude, 1990: "Deep convection and deep water formation. Progress and new directions." EOS, **71(49)**, 1837-1839.

Gill, Adrian E., 1982: *Atmosphere-Ocean Dynamics*. Academic Press, Inc., San Diego, California, 662pp.

Helland-Hansen, B. and F. Nansen, 1909:., *The Norwegian sea, its physical oceanography based upon the Norwegian researches 1900-1904.* Rep. Norw. Fish. Mar. Invest., **2**, 390pp.

Killworth, P.D., 1979: "On chimney formations in the deep ocean." J. Phys. Oceanogr., **9**, 531-554.

Koltermann, K.P. and H. Luthje, 1989: *Hydrographic Atlas of the Greenland Sea and Northern Norwegian Seas (1979-1987).* Deutsches Hydrographisches Institut, Hamberg, Germany, 274pp.

Kraus, E.B. and J.S. Turner, 1967: "A one-dimensional model of the seasonal thermocline: II. The general theory and its consequences." Tellus, **19**, 98-106.

Lazier, J.R.N., 1973: "The renewal of Labrador sea water." Deep Sea Research, **20**, 341-353.

Levitus, S., 1982: *Climatological atlas of the world ocean.* National Oceanic Atmospheric Administration Professional Paper 13. Washington, D.C.: Government Printing Office, 173pp.

Maykut, G.A., 1985: *An introduction to ice in the polar oceans APL-UW 8510, 2nd printing.* Dept. of Atmos. Sciences/Geophysics Program, Univ. of Washington. Seattle, Washington, 107pp.

McDougall, T.J., 1984: "The relative roles of diapycnal and isopycnal mixing on subsurface water-mass conversion." J. Phys. Oceanogr., **14**, 1577-1589.

McDougall, T.J., 1987: "Thermobaricity, cabbeling and water-mass conversion." J. Geophys. Res., **92**, 5448-5464.

Millero, F.J., 1978: "Freezing point of sea water." In "Eighth Report of the Joint Panel on Oceanographic Tables and Standards," UNESCO Tech. Pap. Mar. Sci. No. 28, Annex 6. UNESCO, Paris.

Millero, F.J. and A. Poisson, 1981: "International one-atmosphere equation of the state of seawater." Deep Sea Research, **28A**, 625-629.

Mosby, H., 1959: "Deep water in the Norwegian Sea." Geofys. Publ., **21**, 62pp.

Nansen, F., 1906: *Northern waters: Captain Roald Amundsen's oceanographic observations in the Arctic Seas in 1901.* Vid.-Selskap Skrifter. I. Mat.-Naturr. Kl., Dybwad, Christiania 1, (193). 145pp.

Quadfasel, D. and M. Ungewib, (1988): "Mizex 87 - RV VALDIVIA cruise 54. CTD observations in the Greenland Sea, Technical Report 5-88" (unpublished manuscript).

Riehl, H. 1979: *Climate and Weather in the Tropics.* Academic Press., New York, 611 pp.

Rudels, B., 1989: "Greenland sea convection in the winter of 1987-1988." J. Geophys. Res., **94**, 3223-3226.

Scott, J.C. and P.D. Killworth, 1991: "Upper ocean structures in the south-western Iceland sea - A preliminary report." *Deep Convection and Deep Water Formation in the Oceans.* Ed. P.C. Chu and J.C. Gascard. Elsevier Science Publishing Company Inc., Amsterdam, The Netherlands, 16pp.

BIBLIOGRAPHY

Gordon, A.L., 1978: "Deep Antarctic convection west of the Maud Rise." J. Phys. Oceanogr., **8**, 600-612.

Gordon, A.L. and B.A. Huber, 1990: "Southern ocean winter mixed layer." J. Geophys. Res., **95**, 11, 655-11, 672.

Martinson, D.G., 1990: "Evolution of the southern ocean winter mixed layer and sea ice: Open ocean deep water formation and ventilation." J. Geophys. Res., **95**, 11,641-11,654.

Stommel, H., 1972: "Deep winter-time convection in the western Mediterranean Sea." *Studies in Physical Oceanography, A Tribute to George Wust on his 80th Birthday*, Vol. 2, Ed. A.L. Gordon, Gordon and Breach, New York, 207-218.

INITIAL DISTRIBUTION LIST

1.	Defense Technical Information Center Cameron Station Alexandria, VA 22304-6145	2
2.	Library, Code 52 Naval Postgraduate School Monterey, CA 93943-5000	2
3.	Chairman (Code OC/Co) Department of Oceanography Naval Postgraduate School Monterey, CA 93943-5000	1
4.	Chairman (Code MR/Hy) Department of Meteorology Naval Postgraduate School Monterey, CA 93943-5000	1
5.	Dr. Roland W. Garwood (Code OC/Gd) Department of Oceanography Naval Postgraduate School Monterey, CA 93943-5000	1
6.	Dr. Peter C. Chu (Code OC/Cu) Department of Oceanography Naval Postgraduate School Monterey, CA 93943-5000	1
7.	Ms. Arlene Guest (Code OC/Gt) Department of Oceanography Naval Postgraduate School Monterey, CA 93943-5000	1
8.	LCDR James M. Olson 1245 Hickory Nut Drive California, MD 20619	1

9. Commanding Officer — 1
Naval Oceanographic Office
Stennis Space Center
MS 39522-5001

10. Commanding Officer — 1
Fleet Numerical Oceanography Center
Monterey, CA 93943-5005

11. Commanding Officer — 1
Naval Oceanographic and Atmospheric
Research Laboratory
Stennis Space Center
MS 39529-5004

12. Office of Naval Research (Code 420) — 1
Naval Ocean Research and Development
Activity
800 N. Quincy Street
Arlington, VA 22217

13. Library — 1
Scripps Institution of Oceanography
P.O. Box 2367
La Jolla, CA 92037